MOLECULAR BIOLOGY

SUMO-activated target traps (SATTs) enable the identification of a comprehensive E3-specific SUMO proteome

Daniel Salas-Lloret[1], Nicolette S. Jansen[1]†, Easa Nagamalleswari[2]†, Coen van der Meulen[1]‡, Ekaterina Gracheva[1], Arnoud H. de Ru[3], H. Anne Marie Otte[3], Peter A. van Veelen[3], Andrea Pichler[2,4], Joachim Goedhart[5], Alfred C.O. Vertegaal[1], Román González-Prieto[1,6,7]*

Ubiquitin and ubiquitin-like conjugation cascades consist of dedicated E1, E2, and E3 enzymes with E3s providing substrate specificity. Mass spectrometry–based approaches have enabled the identification of more than 6500 SUMO2/3 target proteins. The limited number of SUMO E3s provides the unique opportunity to systematically study E3 substrate wiring. We developed SUMO-activated target traps (SATTs) and systematically identified substrates for eight different SUMO E3s, PIAS1, PIAS2, PIAS3, PIAS4, NSMCE2, ZNF451, LAZSUL (ZNF451-3), and ZMIZ2. SATTs enabled us to identify 427 SUMO1 and 961 SUMO2/3 targets in an E3-specific manner. We found pronounced E3 substrate preference. Quantitative proteomics enabled us to measure substrate specificity of E3s, quantified using the SATT index. Furthermore, we developed the Polar SATTs web-based tool to browse the dataset in an interactive manner. Overall, we uncover E3-to-target wiring of 1388 SUMO substrates, highlighting unique and overlapping sets of substrates for eight different SUMO E3 ligases.

INTRODUCTION

Protein fate and function is controlled by numerous posttranslational modifications (PTMs). Among them, ubiquitination is the second most important PTM after phosphorylation (*1*) and controls virtually every process in eukaryotic cells in a dynamic manner. Ubiquitination consists of the covalent attachment of the small 76 amino acids ubiquitin protein to acceptor proteins and is performed by an enzymatic cascade in which ubiquitin-activating enzymes (E1) activate ubiquitin and transfer it to a ubiquitin-conjugating enzyme (E2), which conjugates ubiquitin to the substrate assisted by a ubiquitin-ligase enzyme (E3). E3s are responsible for determining substrate specificity. The human genome encodes for two ubiquitin E1s, 30 to 40 E2s and more than 600 E3s (*2*).

Similar to ubiquitin, other ubiquitin-like (Ubl) modifiers exist, which have dedicated E1-E2-E3 enzymatic cascades. Among these Ubls, small ubiquitin-like modifiers (SUMOs) are the most abundant ones after ubiquitin. In vertebrates, there are three different types of active SUMOs: SUMO1, SUMO2, and SUMO3. Mature SUMO2 and SUMO3 differ only in a couple of amino acids and are commonly referred to as SUMO2/3. In contrast to ubiquitin, vertebrates express a single E1, a single E2, and less than a dozen bona fide E3s for SUMOs (*2*).

Recent advances in mass spectrometry (MS) technologies and the optimization of sample preparation methodologies (*3*) have enabled the identification of several tens of thousands of acceptor sites on thousands of proteins in human cells both for ubiquitin and SUMOs (*4*–*10*). However, our knowledge on E3 substrate wiring is still very limited. Determining which E3 modifies which substrate is a major challenge.

For ubiquitin, given the high number of E3s, solving the E3-to-target wiring in a proteome-wide manner is virtually impossible. However, for SUMOs, the E3 complexity is limited, simplifying this task. A proposed approach has been the quantification of changes on the SUMO proteome after SUMO E3 overexpression (*11*), which, in principle, is an indirect measure. Another applied approach has been the performance of SUMOylation assays on protein array–based screens (*12*), which is an ex vivo system that misses out on the restricted subcellular localization of proteins and lacks protein-protein complexes that are abundant in cells.

Here, we took advantage of our previous experience in the systematic identification of ubiquitination substrates using ubiquitin-activated interaction traps (UbAITs) (*13*) in the targets of ubiquitin ligase identified by proteomics (TULIP) methodologies (*14*–*16*) and applied it for the identification of SUMO E3-specific substrates in a systematic manner for SUMO E3s in a proteome-wide approach.

RESULTS

SUMO E3 overexpression causes SUMO2/3 depletion in an RNF4-dependent manner

Aiming to identify putative E3-specific SUMOylation substrates, we used a similar approach as previously done with PIAS1 (*11*). We made green fluorescent protein (GFP)–tagged constructs for different SUMO E3s, including NSMCE2, PIAS1, PIAS2, PIAS3, PIAS4, ZNF451, the LAP2α isoform of the ZNF451 SUMO ligase (LAZSUL) and, in addition, another PIAS-like enzyme, ZMIZ2 (*17*–*20*) (Fig. 1A), which we previously tested for in vitro SUMO E3 activity both for SUMO1 and SUMO2 (Fig. 1B). As a result,

[1]Cell and Chemical Biology, Leiden University Medical Center, Leiden, Netherlands. [2]Max Plank Institute for Immunobiology and Epigenetics, Freiburg, Germany. [3]Center for Proteomics and Metabolomics, Leiden University Medical Center, Leiden, Netherlands. [4]Institute of Biochemistry, ETH Zürich, Zürich, Switzerland. [5]University of Amsterdam, Amsterdam, Netherlands. [6]Andalusian Center for Molecular Biology and Regenerative Medicine (CABIMER), Universidad de Sevilla-CSIC-Universidad-Pablo de Olavide, Sevilla, Spain. [7]Departamento de Biología Celular, Facultad de Biología, Universidad de Sevilla, Sevilla, Spain.
*Corresponding author. Email: roman.gonzalez@cabimer.es
†These authors contributed equally to this work.
‡Present address: Rheumatology, Leiden University Medical Center, Leiden, Netherlands.

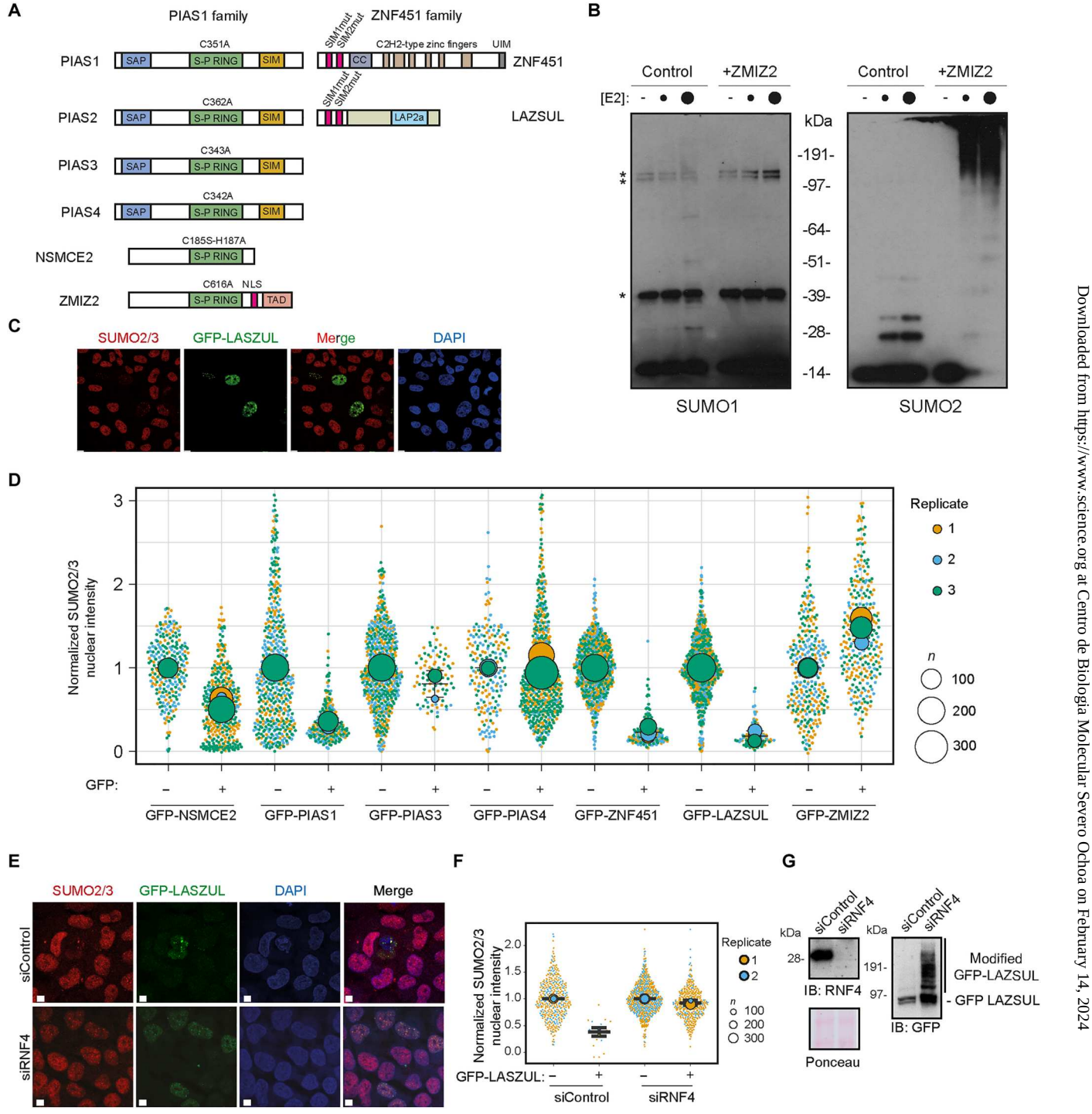

Fig. 1. SUMO E3 overexpression affect endogenous SUMO2/3 levels. (**A**) E3s studied in this article. The mutations performed on each E3 to construct the catalytic dead mutant controls are indicated. (**B**) In vitro SUMOylation assays including ZMIZ2 SUMO E3 enzyme and different concentrations of the SUMO E2. Assays were carried out using either SUMO1 or SUMO2. (**C**) Representative immunofluorescence image of U2OS cells transiently transfected with green fluorescent protein (GFP)–LAZSUL immunostained for SUMO2/3. (**D**) Superplot depicting relative SUMO2/3 nuclear intensities after immunostaining of individual U2OS cells transiently transfected with GFP-tagged constructs of different E3s. Values were normalized to the average SUMO2/3 nuclear intensity of GFP negatives from each individual experiment. Values from three independent experiments are depicted. (**E**) Stable-inducible GFP-LAZSUL–expressing U2OS cells were treated with control or RNF4-targeting small interfering RNAs (siRNAs). Thirty-six hours after siRNA transfection, GFP-LAZSUL expression was induced with doxycycline (20 μg/ml). Cells were fixed 48 hours after siRNA transfection and analyzed by immunostaining. (**F**) Quantification of the normalized nuclear SUMO2/3 intensities from the cells in (E). Independent values from two independent experiments are depicted. (**G**) Analysis by immunoblotting of the cells in (C). Size bars in fluorescence microscopy images represent 10 μm. DAPI, 4′,6-diamidino-2-phenylindole; IB, immunoblot; SIM, SUMO interaction motifs; SAP, SAF-A/B, Acinus and PIAS domain; S-P RING, Siz/Pias Really Interesting New Gene; TAD, Trans Activator Domain; UIM, Ubiquitin Interacting Motif.

we observed that ZMIZ2 has E3 enzymatic activity for SUMO2 but not for SUMO1. Next, we transfected the GFP-tagged constructs of the E3s indicated in Fig. 1A in U2OS cells. To evaluate the transfection efficiency of our constructs, we analyzed our cells by fluorescence microscopy after immunostaining for SUMO2/3 (Fig. 1C and fig. S1A). GFP-positive cells could be observed for every construct at different efficiencies, except for GFP-PIAS2, which transfection did not lead to the appearance of GFP-positive cells. Unexpectedly, the immunofluorescence SUMO2/3 signal was highly reduced in GFP-positive cells for NSMCE2, PIAS1, ZNF451, and LAZSUL (Fig. 1C and fig. S1A). Therefore, we quantified the SUMO2/3 signal by immunofluorescence for GFP-positive and GFP-negative cells from three independent experiments (Fig. 1D). While GFP-NSMCE2, GFP-PIAS1, GFP-PIAS3, GFP-ZNF451, and GFP-LAZSUL reduced the average SUMO2/3 nuclear signal by 41, 63, 19, 77, and 82%, respectively. GFP-PIAS4–positive cells presented a slight increase of 4% in SUMO2/3 signal, and, interestingly, GFP-ZMIZ2 positive cells had a remarkable 46% increase in SUMO2/3 signal.

In a previous screen for targets of the SUMO-targeted ubiquitin ligase (STUbL) RNF4, we observed that SUMO E3s were targets of RNF4 for ubiquitination and subsequent degradation by the proteasome, with ZNF451 and PIAS1 being the strongest RNF4 ubiquitination targets and PIAS4 the weakest. ZMIZ2 was not a substrate for RNF4 (*15*, *16*). We hypothesized that overexpression of these E3s was promoting their hyperactivation, leading to their auto-SUMOylation and increased SUMOylation of their substrates and subsequent degradation in an RNF4-dependent manner. Thus, proteasome inhibition should rescue the effect on SUMO2/3 levels in response to the different E3s overexpression. Therefore, we compared the effect on SUMO2/3 levels of the different SUMO E3s overexpression in the presence or absence of the proteasome inhibitor MG132 for 5 hours (fig. S1B). The 5-hour MG132 treatment could rescue the effect on SUMO2/3 levels of the E3s, which overexpression had milder phenotypes, namely, NSMCE2, PIAS3, and PIAS4, but was not sufficient to rescue strong effects of PIAS1, ZNF451, and LAZSUL overexpression. Furthermore, proteasome inhibition by MG132 has many pleiotropic effects.

To further test our hypothesis in a more specific manner, we made stable inducible U2OS cells for GFP-LAZSUL, which was the E3 with the strongest phenotype (Fig. 1, C and D, and fig. S1, A and B). We treated the cells with a control or an RNF4-targeting small interfering RNA (siRNA), induced the expression of the GFP-LAZSUL construct, and analyzed the cells by immunostaining (Fig. 1, E and F) and immunoblotting (Fig. 1G). RNF4 knockdown caused an increase in the fraction of GFP-LAZSUL–positive cells and rescued the SUMO2/3 depletion phenotype. Consistently, RNF4 knockdown increased the levels of both modified and non-modified GFP-LAZSUL.

RNF4 knockdown increases cellular SUMO2/3 levels but does not affect SUMO1 levels (*21*). Thus, we also decided to investigate the effect of NSMCE2, PIAS1, ZNF451, and LAZSUL transient overexpression on SUMO1 levels by immunofluorescence (fig. S1, C and D). Accordingly, the overexpression of these E3s did not cause SUMO1 depletion as previously observed for SUMO2/3, except for a modest reduction of SUMO1 levels upon LAZSUL overexpression (Fig. 1, C to F).

We conclude that SUMO E3 overexpression–based screens to identify SUMOylation substrates could potentially be misleading due to a negative control loop mediated by RNF4. This loop is activated upon SUMO E3 overexpression and leads to SUMO2/3 depletion in cells. Therefore, SUMO E3 overexpression screens must be carefully evaluated.

SATTs enable to identify an E3-specific SUMO proteome

Previously, in an effort to identify E3-specific ubiquitin substrates, UbAITs were engineered (*13*), which we later adopted and optimized for systematic screening in the TULIP methodology (*15*, *16*). However, because of the high number of ubiquitin E3 enzymes in the human proteome, performing the TULIP methodology on each E3 is an incredibly challenging task.

In contrast to ubiquitin, the number of bona fide SUMO E3 enzymes is more limited, comprising the Siz/Pias Really Interesting New Gene (S-P RING) family, the ZNF451 family, and RANBP2 (*2*). Therefore, addressing the E3 substrate wiring for SUMO E3s is a more manageable challenge.

Thus, similar to the TULIP2 methodology (*15*), we designed the SUMO-activated target traps (SATTs) approach, in which lentiviral doxycycline-inducible plasmids consisting of 10xHIS tag and a gateway cloning sequence, followed by 10xHIS and either mature SUMO1 or mature $SUMO2_{Q87R}$ were constructed (Fig. 2A). The gateway sequence enables the straightforward shuttling of any SUMO E3 of interest. The $SUMO2_{Q87R}$ mutation facilitates the identification of SUMO acceptor sites by MS-based proteomics (*7*, *8*). Consistently, the rationale behind this approach is that, if we generate a linear fusion between an E3 and activated SUMO, the E3 will be prone to use the attached SUMO moiety to modify its substrate, enabling the copurification of the E3 together with its substrate and subsequent identification by MS-based proteomics. In line with TULIP2 methodology (*15*), we included two different negative controls in our screens. The first control is a ΔGG construct where the SUMO moiety lacks the C-terminal di-Gly motif and thus cannot be conjugated to a substrate. The second control is a catalytic dead mutant where the interaction with the SUMO E2 enzyme is abolished, thus the transfer of the SUMO moiety from the E2 to the substrate cannot be catalyzed (Fig. 2B).

Accordingly, we built SATTs for the E3s indicated in Fig. 1A. SUMO1 SATTs for the S-P RING SUMO E3 enzymes, PIAS1, PIAS2, PIAS3, PIAS4, and NSMCE2. In addition, for SUMO2 SATTs, in addition to the S-P RING SUMO E3 enzymes, we also included ZNF451, LAZSUL, and ZMIZ2 as they are exclusive for SUMO2/3 (fig. S2A) (*22*, *23*). Other characterized SUMO E3s were not included for different reasons. RANBP2 was left out from our screen due to the size of the protein (3224 amino acids). Also, the ZNF451 family E3 KIAA1586 was left out because it is exclusively found in primates and not in other vertebrates (*23*). To generate the catalytic dead mutant controls, we introduced specific mutations in each E3 (Fig. 1A). For the S-P RING family E3s, we mutated cysteines in the S-P RING domain, and for the ZNF451 family E3s, we mutated the SUMO interaction motifs by substituting the long hydrophobic amino acids into alanines (*23*).

Next, we constructed U2OS cells expressing HIS-SUMO1 or HIS-$SUMO2_{Q87R}$ in a constitutive manner or stably expressing the inducible E3 SATTs constructs indicated in fig. S2A, including the ΔGG and catalytic dead mutant–negative controls. We induced the expression of the constructs for 24 hours, lysed the cells in denaturing conditions, and purified the SATT conjugates from four independent biological repeats (five in the case of ZMIZ2), yielding

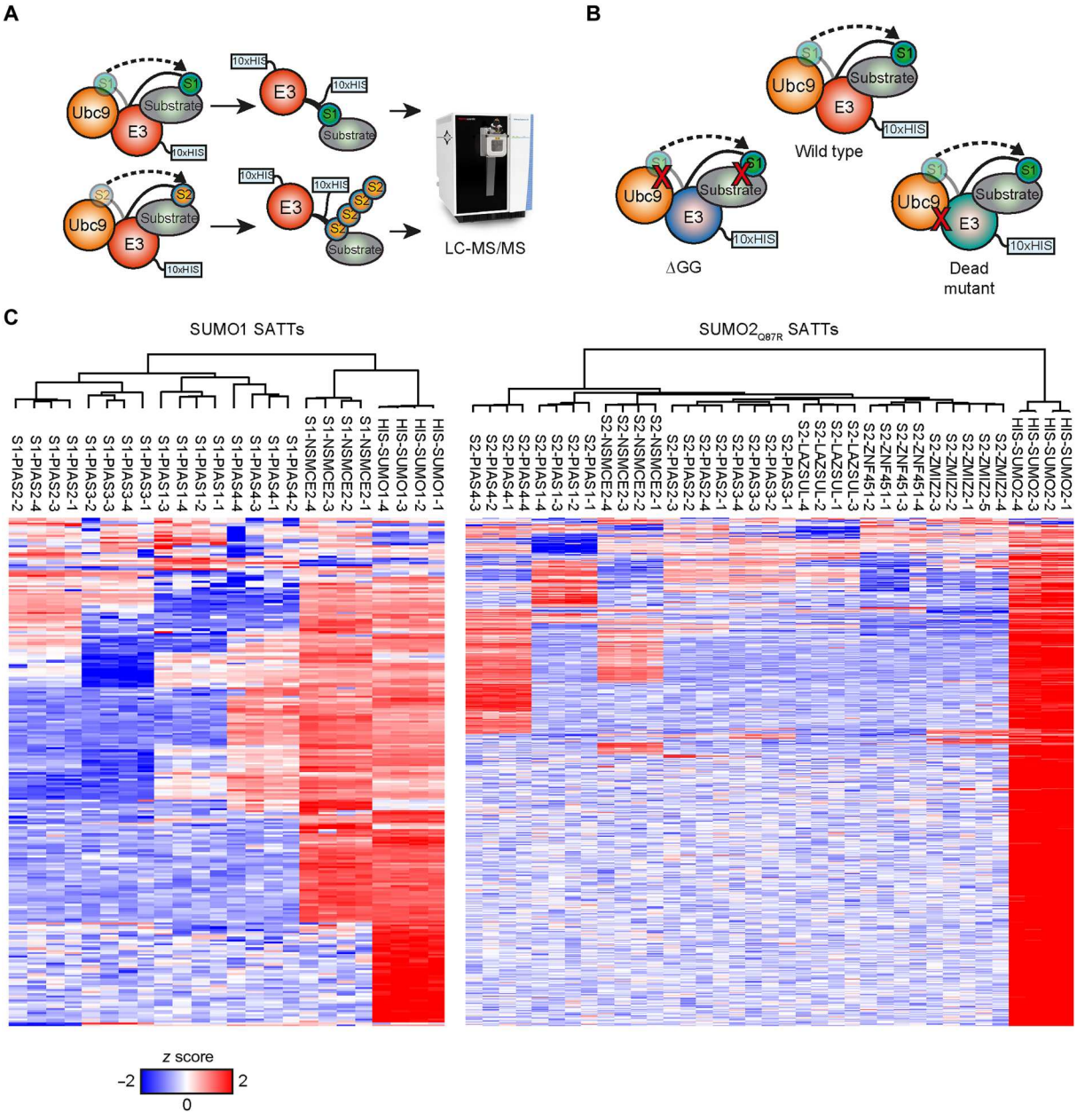

Fig. 2. SUMO-activated target traps (SATTs) enable the identification of E3-specific SUMOylatio substrates. (**A**) SATTs screen rationale. SUMO moieties covalently attach to the C-term of an E3 of interest, which will be attached to E3 substrates, enabling the copurification of the E3 together with the SUMOylation target, which will be later identified by mass spectrometry (MS). (**B**) SATT negative controls rationale. While ΔGG SATTs lack the C-terminal SUMO diGly motif, unable to conjugate to the substrate, catalytic dead mutants prevent interaction with the SUMO E2. (**C**) Heatmap of *z* scores for different SATT targets. Only HIS-SUMO1 and HIS-SUMO2$_{Q87R}$ targets are included. LC-MS/MS, liquid chromatography tandem MS.

a total of 171 samples. To avoid RNF4-mediated degradation of the SATTs due to auto-SUMOylation (Fig. 1) and to increase the number of SUMOylation conjugates (*8*), the proteasome was inhibited for 5 hours with MG132.

Sample analysis by immunoblotting (fig. S2, B and C) showed that the expression levels of the SATTs were below or close to endogenous counterparts for every construct. Moreover, signal could be observed in a higher–molecular weight smear for the wild type and catalytic dead mutant construct for every SATT, corresponding to E3-SUMO-target conjugates. This smear was absent in the ΔGG constructs. Consistently, the catalytic dead SATT smears had different profiles than their wild-type counterparts, indicating that the SUMO moieties in the mutant SATTs could still be used for conjugation by other endogenous E3s.

For the cell lines expressing either HIS-SUMO1 or HIS-SUMO2$_{Q87R}$ in a constitutive manner, MS analysis of the samples enabled the identification of 244 SUMO1 targets and 1509 SUMO2 targets (data S1 and S2) after 5 hours of proteasome inhibition with

MG132. Among the 244 SUMO1 targets, 171 could be considered a SUMO1 SATT conjugate for at least one SUMO E3. In the case of SUMO2 SATT conjugates, the numbers were 570 of 1509, which were preferential or specific for the different E3s (Fig. 2C and data S3 and S4). When compared with the biggest SUMO2 target study to date in U2OS cells (*7*), the number of SUMO2 SATT targets that had been identified as SUMO2 targets increased to 656 (data S5).

However, the SUMO proteome is highly diverse, depending on the cell type and experimental conditions of study (*7*). Therefore, we considered the possibility that the SATTs could enable the modification and enrichment of SUMOylation substrates, which are not constitutively modified in the cell line and condition of study or not detectable when a total SUMO proteome purification is performed. Accordingly, we also analyzed the MS data from the SATTs in an unbiased manner. Namely, proteins not considered as HIS-SUMO targets were included when identified as SATT substrates (fig. S3 and data S6 and S7). This way, we could identify 302 extra putative substrates for SUMO1 SATTs, mainly for NSMCE2 and PIAS2, and 459 additional putative substrates for SUMO2 SATTs, mainly for PIAS2 and LAZSUL.

The SATT index measures substrate specificity

Although the substrates we identified for each tested SUMO E3 were relatively specific for every E3 when comparing a wild-type SATT with its ΔGG counterpart, all the substrates did not remain equally significant compared to their catalytic dead mutant counterpart (data S3, S4, S6, and S7), indicating that, as previously shown for UbAITs (*13*, *15*, *16*), the SUMO moiety attached to the mutant SATT can also be conjugated to a substrate by another endogenous SUMO E3.

Therefore, we used the relation between the differences of the enrichment of a substrate for a specific E3 comparing both the ΔGG and the mutant counterpart to wild type, which we termed SATT index

$$SATTi = \frac{[\log_2\ SATT^{WT}] - [\log_2\ SATT^{Mut}]}{[\log_2\ SATT^{WT}] - [\log_2\ SATT^{\Delta GG}]}$$

Values close to 1 and higher are considered very specific, and values close to 0 and lower are considered not specific.

Different E3s have different preferences toward SUMO1 or SUMO2/3

It could be argued that making a SUMO1 SATT with an E3 which normally catalyzes SUMO2/3 conjugation might force SUMO1 conjugation on a SUMO2/3 substrate. Thus, we decided to investigate if SUMO E3s could discriminate substrate specificity depending on the SUMO type they were conjugating. First, we looked at the overlap between SUMO1 and SUMO2 substrates (Fig. 3A). Overall, and similar to previous studies, SUMO2 is the most abundant and important SUMO (*10*, *24*). While most of the identified SUMO1 targets (87%) can also be modified by SUMO2/3, only 14% of the SUMO2 substrates can also be modified by SUMO1. Next, we looked at the substrate preference and overlap for the different S-P RING E3s that had been investigated for both SUMO1 and SUMO2 SATTs (Fig. 3B). On one side, in contrast to SUMO proteome data (Fig. 3A), NSMCE2, PIAS1, and PIAS2 data indicated a preference for SUMO1 modification. For PIAS1, only 9% of the SUMO1 substrates were also SUMO2/3 substrates (87% in SUMO proteome), and 45% of the SUMO2/3 were also substrates for SUMO1 (14% in SUMO proteome). This preference was milder for NSMCE2, where the numbers were 63 and 57%, respectively, and PIAS2, 69% for SUMO1, and 23% for SUMO2. For PIAS3 and PIAS4, the preference for SUMO2 modification was more acute than in total SUMO proteome analysis. For PIAS3, there was only one protein identified for SUMO1 conjugation. This protein was also found for PIAS3 SUMO2 conjugation (100%). For PIAS4, 93% of SUMO1 conjugates were also modified by SUMO2. These values indicate that PIAS3 and PIAS4 are mainly a SUMO2/3 E3 enzyme, which is consistent with previous studies on SUMO specificity, and consistently, SUMO1 ligase activity has also been reported to be higher for PIAS1 and PIAS2 (*12*).

Gene Ontology analysis identifies E3s in different biological processes

Gene Ontology analysis for biological processes of the SUMOylation substrates for the different E3s indicated that different E3s are involved in different processes (Fig. 3C and data S8). As expected, PIAS1, PIAS4, NSCME2, and ZNF451 substrates are enriched in Gene Ontology terms relative to genome biology (*25*–*31*), and PIAS3 substrates are enriched for maintenance of proteins at the nucleus (*32*–*34*). LAZSUL highest enrichment term was protein SUMOylation. ZMIZ2 substrates were not enriched for specific cellular processes. PIAS2 substrates are enriched for membrane translocation and adenosine 5′-diphosphate/adenosine 5′-triphosphate (ATP) mitochondrial transport.

PIAS4 and NSMCE2 make hybrid SUMO1-SUMO2/3 chains

$SUMO2_{Q87R}$ SATTs leave a QQTGG remnant after tryptic digestion on acceptor lysines, which can be identified by MS-based proteomics (*8*). Although K11 is known to be the canonical site to make SUMO2/3 chains (*35*), several other SUMO2/3 sites at the endogenous level have been identified (*6*). Therefore, in addition to K11-SUMO2/3 chains, other chain types exist.

MS analysis of our samples enabled us to obtain MS/MS spectra in which the QQTGG remnant could be localized on SUMOs in an unambiguous manner (fig. S4), and the intensity of these SUMOylation sites could be quantified (Fig. 4). SUMO2/3 K11 chains, were found with every E3. As expected, no QQTGG-modified peptides were found in ΔGG SATTs samples. In contrast, signal for the modification with SUMO2/3 on K11 either on SUMO2 or SUMO3 could be detected in every SATT and, at less intense level, on K5. This included both wild-type and catalytic dead mutant SATTs. Only NSCME2 and PIAS4 wild-type SATTs were able to modify SUMO1 with SUMO2/3 at K7, being completely dependent on the catalytic activity of the SATT. Similarly, SUMO3 K7 chains were also formed with NSCME2 and PIAS4 but only depending on the catalytic activity of NSMCE2. Last, SUMO2/3/4 K32/33/33 chains were only detected for NSCME2 and were completely depending on NSMCE2 catalytic activity.

SATTs complement analysis provides an extra comparison

Next, we made statistical comparisons of proteins that were enriched or depleted in the wild-type SATTs samples using all the other wild-type SATTs as a control. This was done both for considering and not considering exclusively the SUMO1 or SUMO2-3

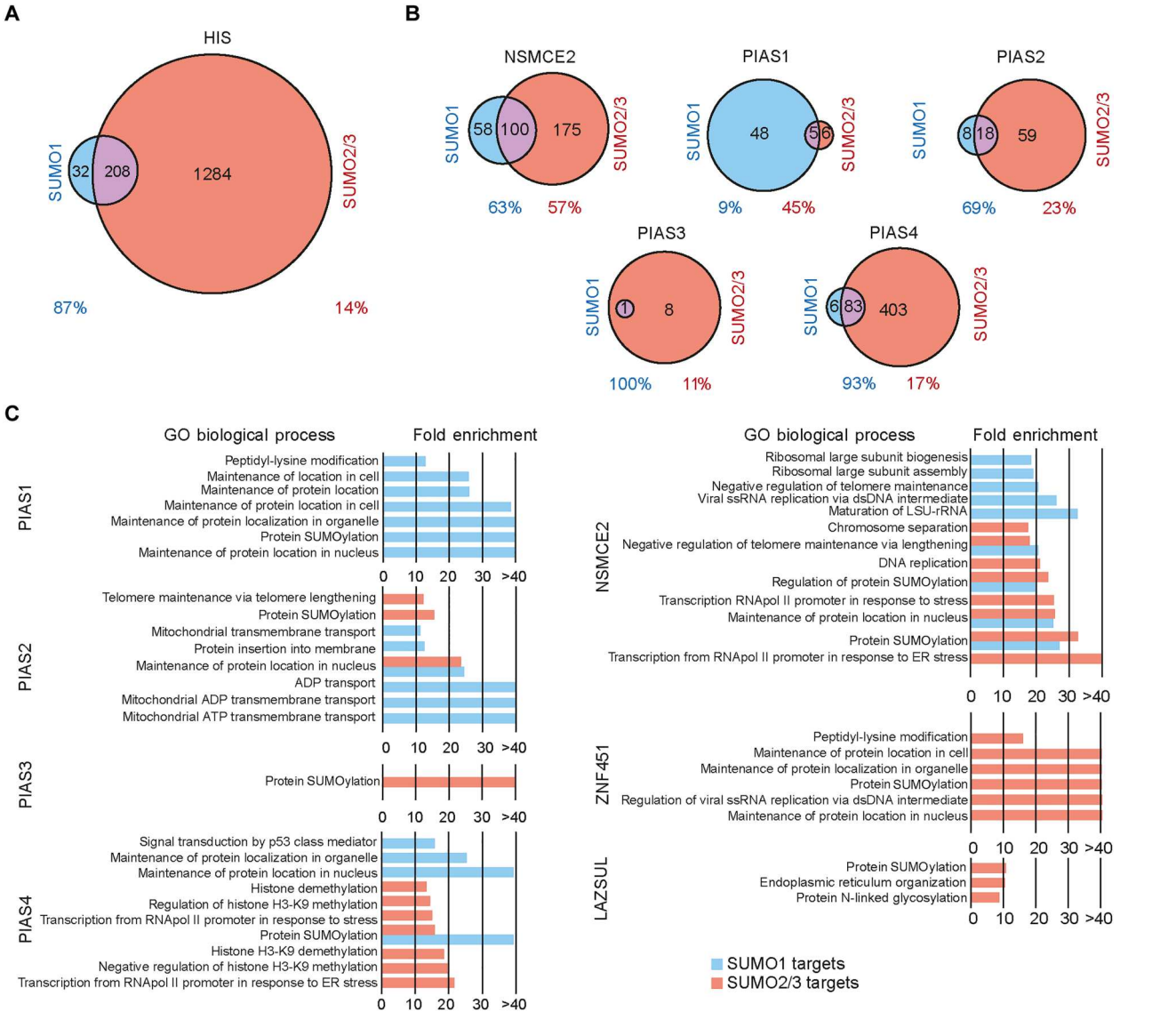

Fig. 3. SUMO1-SUMO2/3 overlap and Gene Ontology. (**A**) Overlap between HIS-SUMO1 and HIS-SUMO2$_{Q87R}$ targets. (**B**) Overlap between SUMO1–SUMO-activated target trap (SATT) and SUMO2-SATT substrates for the indicated E3s. (**C**) Gene Ontology (GO) analysis for the SUMOylation substrates of the different E3 SATTs analyzed in this study. ER, endoplasmic reticulum; ADP, adenosine 5′-diphosphate; ATP, adenosine 5′-triphosphate; LSU-rRNA, large subunit ribosomal–ribonucleic acid; dsDNA, double-stranded DNA.

substrates identified in data S1 and S2 (data S9 to S12, Fig. 5, and fig. S5).

Together, these analyses enabled the identification of very high-confidence E3-specific SUMOylation substrates in which wild-type SATTs target proteins were statistically enriched when compared to their ΔGG and catalytic dead mutant counterparts and compared to all the other wild-type SATTs (data S13).

Polar SATTs is a user-friendly site to browse the dataset

Most proteomic screens, including this one, usually consist of large spreadsheet datasets full of gene/protein names, values, and comparisons. The interpretation of these datasets can be daunting for researchers from other disciplines. To overcome these potential outreach hurdles, we developed an online web application tool to browse the dataset, which is freely accessible (https://amsterdamstudygroup.shinyapps.io/PolaRVolcaNoseR/). This tool enables users to select a protein of interest and, if present in this study, will pop up in a polar plot in the sectors corresponding to the relevant E3s, indicating enrichment in terms of *P* value and difference between wild-type and either ΔGG SATTs or all the other wild-type SATTs as complement control. In addition, for the ΔGG SATTs, how relatively specific the substrate is for the E3 in terms of SATT index is depicted with a color scale.

Moreover, the app can be used to customize the data visualization by enabling adjustment of the *P* value and differences, choosing to hide the values that exceed the limits. The size of the data points can also be adjusted to facilitate visualization, and the resulting

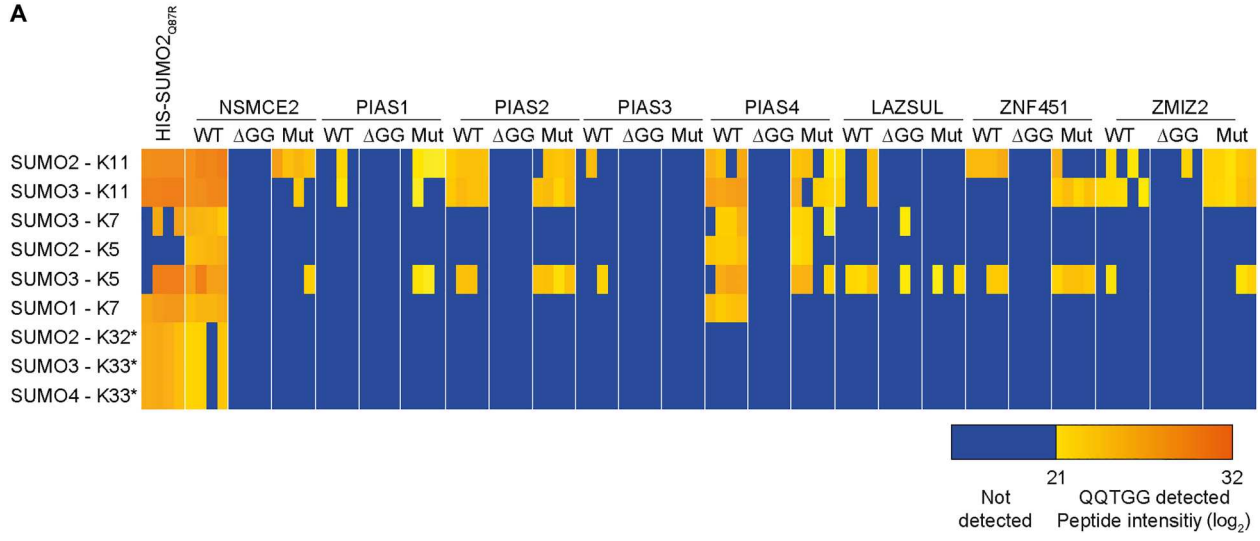

Fig. 4. SUMO-activated target trap (SATT)–specific SUMO chains. (**A**) Total peptide intensities of the different peptides corresponding to different acceptor lysines in SUMO1, SUMO2, SUMO3, and SUMO4 depicted in fig. S4 in the different $SUMO2_{Q87R}$ SATT samples. * indicates that this site corresponds to a peptide present in the three indicated SUMO types, thus not enabling distinction. WT, wild type.

figure highlighting the desired substrates can be exported in .pdf or .png. A "dark theme" is also available.

Last, if users prefer browsing in independent volcano plots instead of the default polar plot, that is also enabled. An example of visualization of different SUMOylation substrates for different E3s using the app is shown in (Fig. 6).

E3 identified substrates can be confirmed by orthogonal validation

Last, we performed orthogonal validation of the identified substrates for some E3 enzymes, including NSMCE2, LAZSUL, and PIAS4. For orthogonal validation of NSMCE2 substrates, we stably expressed or not HIS-$SUMO2_{Q87R}$ in parental and NSMCE2 knockout (NSMCE2-KO) cells (*36*) and rescued NSMCE2-KO with either wild-type NSMCE2 or with a catalytic dead mutant $NSMCE2_{C185S/H187A}$ (*37*). Next, cells were cultured, treated with proteasome inhibitor MG132 as previously done for the SATTs, and lysed for subsequent nickel-nitrilotriacetic (Ni-NTA) purification of the HIS-$SUMO2_{Q87R}$ proteome. MS-based proteomics analysis was performed, and the obtained data were processed together with the NSCME2-SUMO2-SATT data (Fig. 7, A and B, and data S14). Among the statistically significant NSMCE2-SUMO2-SATT substrates compared to both their ΔGG and catalytic mutant counterparts and both in this analysis and analysis from data S4, 31 proteins were considered as putative SUMOylation substrates for both U2OS and NSCME2-KO parental cells. Of those 31 proteins, 10 proteins were statistically reduced in their SUMOylation levels depending on NSMCE2 catalytic activity. Among the 21 proteins, which SUMOylation status was not affected by the lack of NSMCE2 catalytic activity, 17 of them were also strong substrates for other E3 SATTs. Two proteins, namely, ERCC4 and PAF1, were strong substrates for NSMCE2-SUMO2-SATT and had their SUMOylation levels affected by lack of NSMCE2 catalytic activity and were not strong E3 substrates for other SATTs. We decided to analyze these two candidates by immunoblotting (Fig. 7C). Consistently, a big reduction in the SUMOylation signal could be observed when the catalytic activity of NSMCE2 was not present.

In addition, we generated LAZSUL-KO U2OS cells (fig. S6) and stably expressed HIS-SUMO2. The proliferation marker protein Ki-67 had a high SATTi for LAZSUL was identified as a HIS-$SUMO2_{Q87R}$ substrate (data S4). Accordingly, Ki-67 SUMOylation levels were substantially reduced when LAZSUL was not present (Fig. 7D).

In an alternative approach, we performed a short hairpin RNA (shRNA)–mediated knockdown of PIAS4 in parental or HIS-$SUMO2_{Q87R}$ U2OS cells. Analysis by immunoblotting of the HIS-$SUMO_{Q87R}$ proteome validated strong PIAS4-S2-SATT targets with high SATT index value, which had not been previously described in the literature as the histone-lysine *N*-methyltransferase EHMT1 or the transcription factor jun-B (Fig. 7E).

DISCUSSION

This resource identifies 427 SUMO1 and 961 SUMO E3 targets in an E3-specific manner. Nevertheless, while the number of SUMOylation substrates that have been identified in previously published datasets for SUMO1 and SUMO2 in U2OS cells is higher (*7*, *9*, *10*) (data S1 and S2), proteins that have not been previously identified described as SUMOylation substrates upon proteasome inhibition with MG132 were identified as E3 substrates for SUMO conjugation in this work. It is noteworthy that the screens performed in this project only comprised a single condition of 5 hours of proteasome inhibition with MG132 in a single-cell line, U2OS, for eight different SUMO ligases.

The results obtained from this screen also corroborate previous observations on protein arrays regarding E3 preferences for SUMO1 or SUMO2/3 (*12*). PIAS3 and PIAS4 had been proposed to have a big preference for SUMO2. Consistently, for PIAS3, enrichments are much higher in SUMO2 SATTs than in SUMO1 SATTs (Fig. 3B), and for PIAS4, 93% of SUMO1 substrates are shared with SUMO2. PIAS1 was observed to have a more balanced

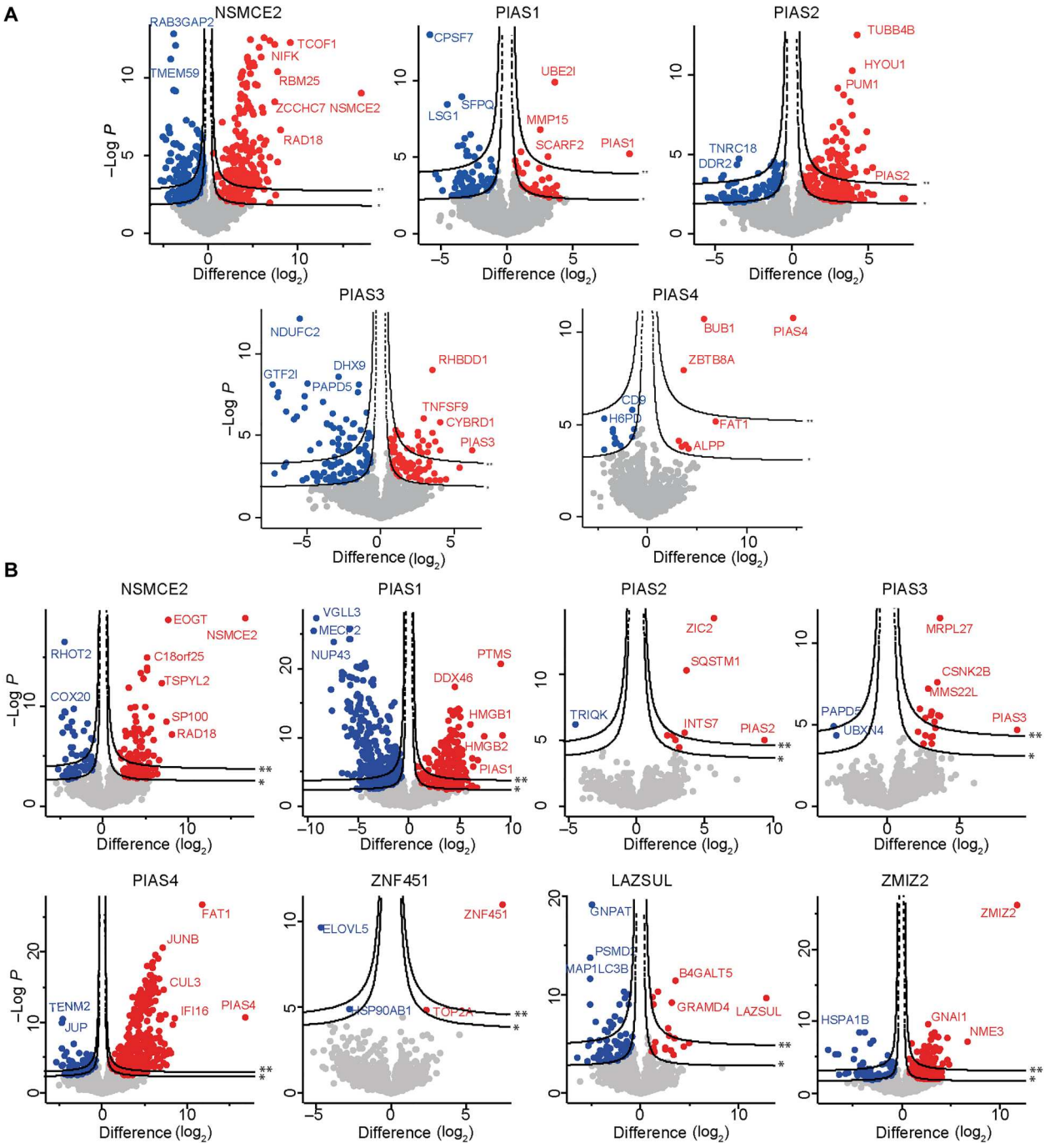

Fig. 5. Complement analysis. Multiple volcano plots (Hawaii plot) depicting statistical differences of different unbiased SUMO1–SUMO-activated target trap (SATT) (**A**) or SUMO2-SATT (**B**) SATT targets using the values from the rest of wild-type SATTs as complement negative control. Cutoffs represent a Pearson of 100 and a false discovery rate = 0.05 (*) or 0.01 (**) and an S0 = 0.1.

preference toward SUMO1, in line with our SATT screen, which showed PIAS1 to be SUMO1 preferential. For PIAS2 and NSMCE2, there is no data available from protein arrays to make this comparison, but they show a more balanced preference toward SUMO1.

In addition, substrates that are highly SUMOylated and shared by every E3, such as PML, RANGAP, RNF216, or ZBTB33, have a very low SATT index for every E3, which indicates that either are redundant substrates can be modified by different E3s or require no E3 at all for SUMOylation (data S1 and S2). Moreover, some substrates with high SATTi values for specific E3s have been previously independently identified as substrates in other laboratories for the relevant E3s. Namely, PARP1 (*38*), ZMYM2 (*39*), and TOP2a (*27*,

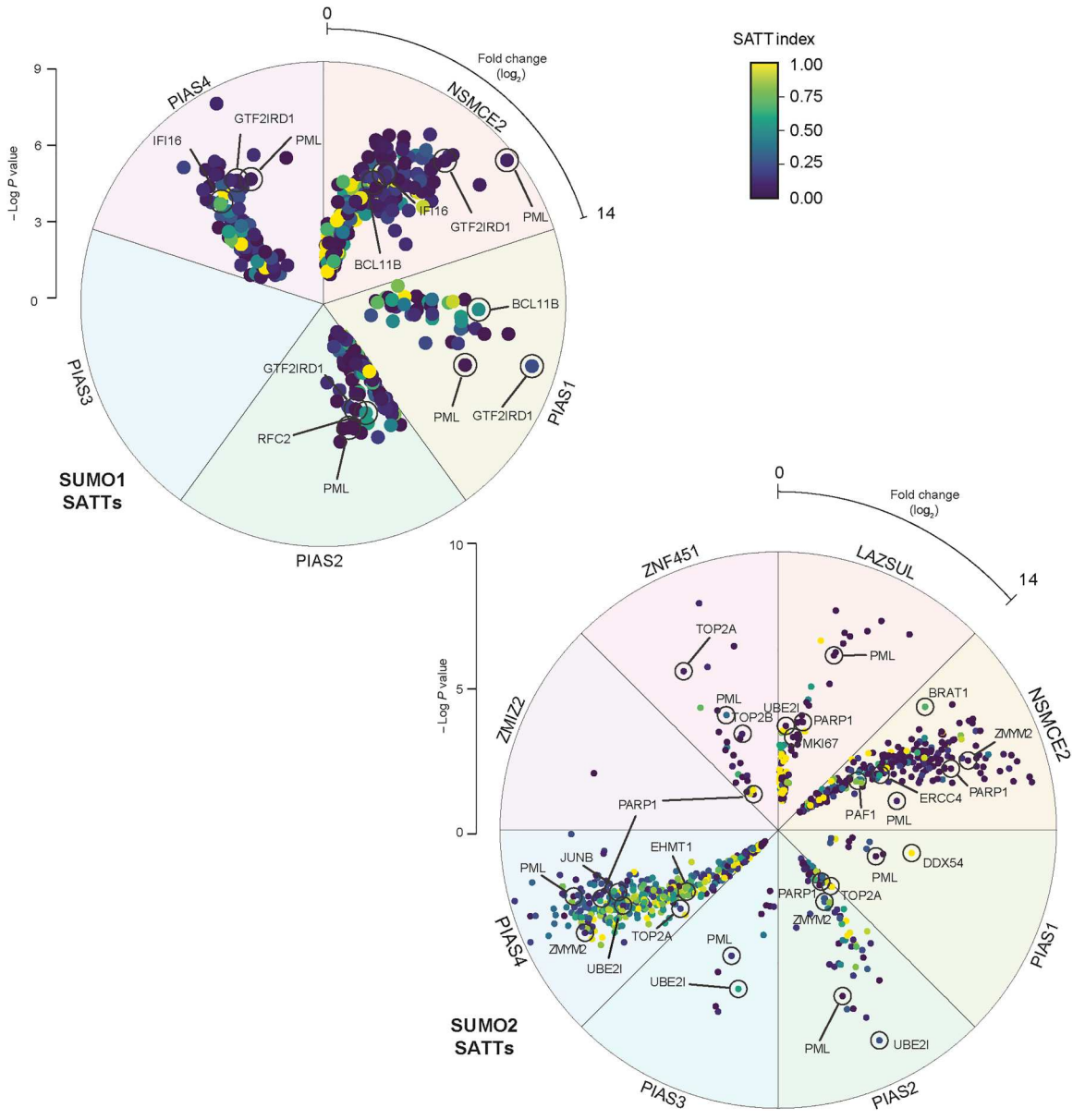

Fig. 6. Polar SUMO-activated target traps (SATTs) application. SATT Polar plots extracted from the polarVolcaNoseR web application. Some of the most prominent or specific substrates from different E3s are indicated. Depicted plots use ΔGG as control, which include the SATT index, and only consider HIS-SUMO targets.

30) for PIAS4 and SUMO2/3 (Fig. 6 and data S4 and S7) as well as SMC5 for NSMCE2 and SUMO1 (*26*) (data S3 and S6).

SUMO2/3 is not recycled at the proteasome

Whereas the classical model suggests that SUMO2/3 is deconjugated and recycled at the proteasome (*40*), we have observed that when overexpressing PIAS1, ZNF451, or LAZSUL, SUMO2/3 is depleted from the nucleus in an RNF4-dependent manner (Fig. 1). This indicates that SUMO2/3 moieties attached to STUbL targets are also degraded. Whether the proteasome discriminates between mixed SUMO2/3-ubiquitin chains on substrates and substrates that are comodified independently by SUMO2/3 and ubiquitin chains requires further investigation. We previously showed that the oncogene c-Myc, which SUMOylated form highly accumulates upon proteasome inhibition and is an RNF4 target (*8*, *15*, *41*), is SUMOylated and ubiquitinated on different residues in an RNF4-dependent manner. On the basis of these results, we favor the hypothesis that independent ubiquitination of the SUMOylated substrate is sufficient for the degradation of SUMO moieties attached to the substrate without the need for mixed chains. Nevertheless, we also found that mixed SUMO/ubiquitin polymers are efficiently stabilized by proteasome inhibitors, indicating that these mixed polymers also constitute an efficient proteasomal degradation signal (*5*).

In contrast to GFP-PIAS1, GFP-ZNF451, GFP-LAZSUL, and, partially, GFP-PIAS3, which overexpression caused nuclear SUMO2/3 depletion, GFP-PIAS4 overexpression was linked to a slight increase in nuclear SUMO2/3 levels (Fig. 1). PIAS4 and NSMCE2 were the only E3s capable of assembling SUMO2/3-

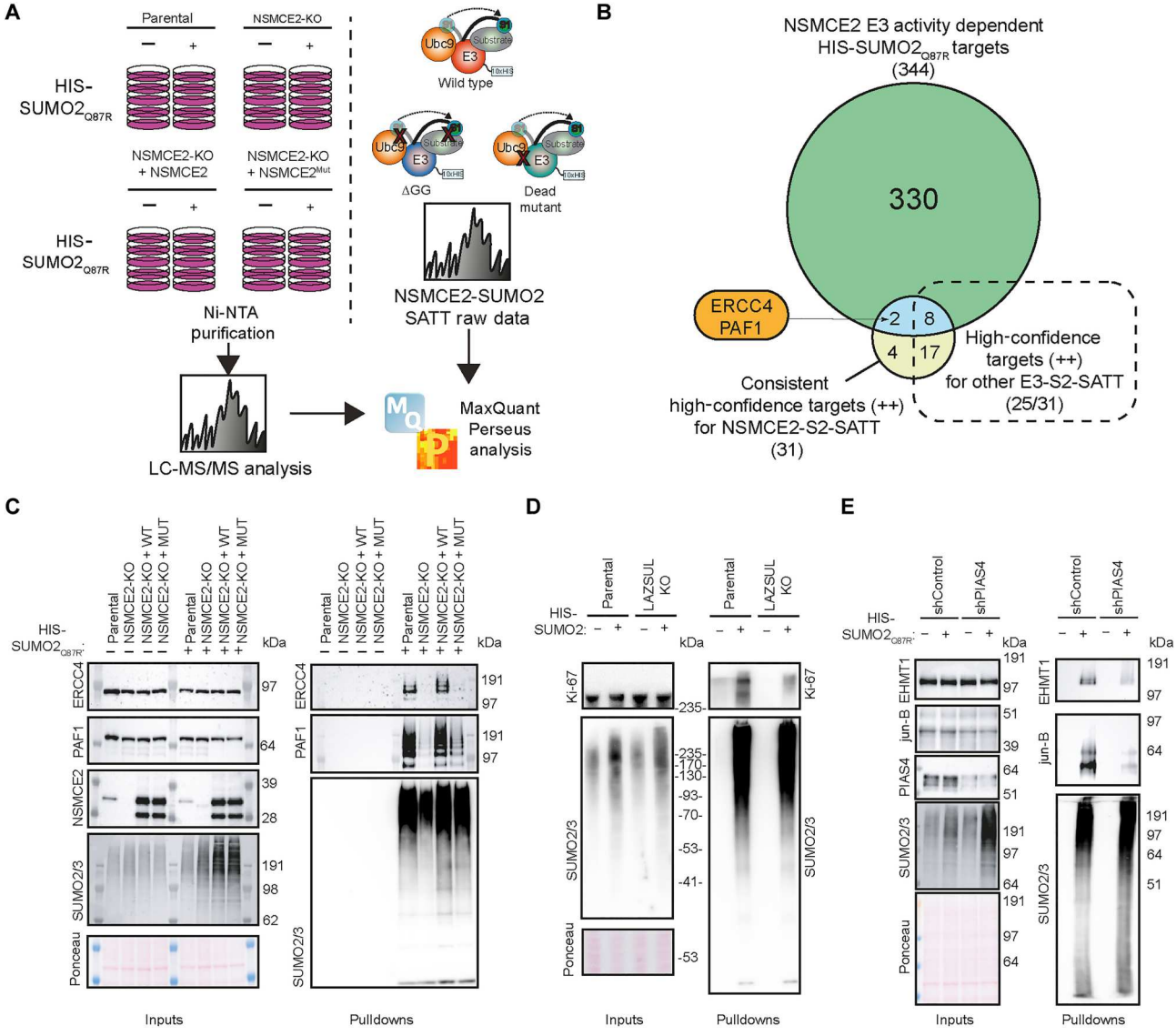

Fig. 7. Orthogonal validation. (**A**) Experimental setup. Parental and NSMCE2–knockout (KO) U2OS cells rescued or not with either wild-type (WT) NSMCE2 or a catalytic dead mutant and expressing or not HIS-SUMO2$_{Q87R}$ were cultured, incubated for 5 hours with MG132, lysed, and analyzed by liquid chromatography tandem mass spectrometry (LC-MS/MS). Next, data were processed together with the NSMCE2-SUMO2–SUMO-activated target trap (SATT)data by MaxQuant and Perseus. (**B**) Venn diagram depicting overlap among NSMCE2-SUMO2-SATT substrates, HIS-SUMO2$_{Q87R}$ substrates affected by lack of NSMCE2 catalytic activity, and NSMCE2-SUMO2-SATT substrates shared with other E3-SATTs. (**C** to **E**) Immunoblot analysis of HIS-SUMO2 substrates decreasing upon NSMCE2 catalytic activity (C), LAZSUL-KO (D), or PIAS4 knockdown (E).

SUMO1 mixed chains (Fig. 4). We therefore hypothesize that SUMO2/3-SUMO1 mixed chains are poor substrates for RNF4. Similarly, SUMO1-capped SUMO2/3 chains are poor substrates for RNF4 but efficient substrates for RNF111/Arkadia, another STUbL (*42*).

Perspective and implications

SUMOylation of proteins occurs in response to many different types of cellular stresses, such as DNA damage or replication stress and heat shock among others (*31*, *43*). The E3 that modifies a specific target may vary depending on the scenario, and SATTs should be screened for specific targets at specific conditions. One E3 can be specific for the SUMOylation of a protein in a certain context and another in a different context. In this regard, PIAS4 and NSCME2 share many SUMOylation substrates from the DNA damage response. We speculate that, while NSMCE2 SUMOylates these substrates in response to DNA damage in the context of DNA replication as part of the SMC5/6 complex (*44*), PIAS4 SUMOylates these substrates in a replication-independent manner.

Moreover, altering the expression levels of different components of the SUMO pathway affects the SUMOylation landscape (*7*, *11*, *45*–*47*). Although here we expressed the SATTs at close-to-endogenous levels or below endogenous levels, this might affect both the SUMOylation status of target proteins, E3 specificity, or SUMO type modification, as proposed in Fig. 3A.

Previously, it was shown that both SUMO1 and SUMO2 were recruited to sites of DNA damage, with SUMO1 recruitment depending on PIAS4 (*25*). Accordingly, DNA damage repair pathways are significantly enriched among PIAS4 substrates for SUMO1 (data S8). However, we did not detect affinity of DNA damage response–related proteins for SUMO1 moieties (*10*). This might indicate that SUMO1 moieties incorporated at DNA damage sites in a PIAS4-dependent manner correspond to hybrid SUMO1-SUMO2/3 chains. Our results indicate that different types of mixed SUMO polymers and mixed SUMO/ubiquitin polymers constitute differential signals.

Nonetheless, results from this screen might open not previously explored lines of investigation. Gene Ontology analysis revealed that PIAS2 substrates are significantly enriched for serine import into mitochondrion (Fig. 3B) as biological function, which deregulation has been very recently described as causative for Parkinson's disease (*48*). PIAS2 has also been recently linked to parkinsonism (*49*). This suggests a potential role for the identified PIAS2 substrates in the development of this neurological disorder. Future mining of the resource presented here could improve our understanding of the biological functions of the different SUMO E3 ligases.

MATERIALS AND METHODS

Antibodies

Antibodies are listed in table S1 with working dilutions. Rabbit polyclonal anti–ZNF451-3 (LAZSUL) antibodies were raised against recombinant full-length human ZNF451-3 (*23*) and injected in rabbits by Cambridge Research Biochemicals (United Kingdom). Subsequent affinity purification was against recombinant full-length ZNF451-3 (LAZSUL).

Generation of SATT toolbox

For the generation of the SATTs plasmids, AgeI-10HIS-SUMO1-XmaI, AgeI-10HIS-SUMO1ΔGG-XmaI, AgeI-10HIS-SUMO2$_{Q87R}$-XmaI, and AgeI-10HIS-SUMO1ΔGG$_{Q87R}$-XmaI restriction fragments from polymerase chain reaction (PCR) products amplified with primers FW-AgeI-10HIS-SUMO1, FW-AgeI-10HIS-SUMO2, RV-XmaI-SUMO1, RV-XmaI-SUMO1noGlyGly, RV-XmaI-SUMO2-Q87R, and RV-XmaI-SUMO2-Q87R-noGlyGly, were cloned into AgeI-SpeI sites of pCW57.1-nonStop plasmid (*16*). The N-terminal 10xHIS tag was cloned as previously done for the H-TULIP2 plasmids (*15*). Primer sequences are listed in table S2.

Generation of lentiviral plasmids

SUMO1 and SUMO2$_{Q87R}$ SATT plasmids containing a SUMO E3 ligase of interest were generated using gateway cloning LR reaction (Thermo Fisher Scientific). LR reactions were performed using a donor plasmid containing an E3 enzyme complementary DNA (cDNA) without stop codon and a SATT plasmid as destination vector. We used different donor plasmids: pENTR223-PIAS1, pDNOR221-PIAS2, pENTR223-PIAS3, pDNOR221-PIAS4, pENTR223- NSMCE2, and pENTR233-ZMIZ2 were obtained from DNASU plasmid repository with the following IDs: HsCD00505402, HsCD00042133, HsCD00514170, HsCD00041383, HsCD00287670, and HsCD00505806, respectively. pDNOR207-ZNF451-1 (isoform 1), pDNOR207-ZNF451-3 (LAZSUL), and pDNOR207-GPF-ZNF451-3 were generated using the gateway cloning BP reaction (Thermo Fisher Scientific) upon cDNA amplification using BP-tailed primers and pDNOR207 as donor vector. Catalytic dead mutants of each SUMO E3 ligase were generated by site-directed mutagenesis on donor plasmids and subsequent LR reaction into SATT plasmids. Primer sequences are listed in table S2.

Stable-inducible GFP-LAZSUL construct was generated by LR gateway cloning between pDNOR207-GFP-ZNF451-3 and pCW57.1 (Addgene, #41393). NSMCE2-rescued constructs were generated by LR between either pENTR223-NSMCE2-WT or pENTR223-NSMCE2$_{C185S-H187A}$ and pLX303 (Addgene, #25897).

Transfection of GFP-E3 constructs

For the transient transfection experiments of GFP-tagged SUMO E3 ligases in Fig. 1 and fig. S1, approximately 10,000 U2OS cells were transferred to six-well plates containing 18-mm coverslips and left to attach overnight. The next day, 300 μl of transfection mixture consisting of 150 mM NaCl containing 1 μg of plasmid DNA and 6 μg of polyethyleneimine (PEI) were added to the cells. Twenty-four hours after transfection, culture medium was replaced for fresh medium. Cells were fixed with 1% paraformaldehyde 48 hours after transfection for immunofluorescence analysis.

Generation of LAZSUL-KO cell lines

Three different gRNAs targeting LAZSUL exon 4 start and LAP2a domain (table S2) were cloned, independently, into a Cas9-GFP–containing pX458 backbone plasmid (Addgene, #48138). U2OS cells were seeded in plates with a diameter of 15 cm at 10% confluency and left to attach overnight. The next day, 2 ml of transfection mixture consisting of 150 mM NaCl containing 5-μg DNA of each plasmid and 100 μg of polyethylenimine was added to the cells. Transfection medium was replaced by fresh culture medium after 24 hours. Forty-eight hours after transfection, cells were GFP fluorescence-activated cell sorting (FACS)–sorted by FACSAria III (BD Biosciences) and seeded for monoclonal expansion.

Selection of positive clones was performed by genomic PCR and immunoblotting (fig. S6). Two primers targeting the LAP2a coding sequence were used for clones validation by genomic PCR (table S2). Six of 30 clones were found positive with a 972–base pair deletion in the LAP2a-coding sequence (fig. S6A). Parental and clone 27 LAZSUL-KO cell lines were subjected to immunoblotting against a taylored LAZSUL antibody (table S1 and fig. S6B).

siRNA transfection for RNF4 knockdown

siRNA-mediated knockdowns were performed as previously described (*16*). DharmaFECT 1 transfection reagent (GE Life Sciences) was used, according to the manufacturer's instructions, using on-target plus RNF4 siRNAs (J-006557-08) and the nontargeted control siGENOME non-targeting siRNA #1 (GE Life Sciences).

Lentivirus production

Human embryonic kidney (HEK) 293T cells were seeded at 30% confluency in a T175 flask containing 16 ml of Dulbecco's modified Eagle's medium (DMEM) + 10% fetal bovine serum (FBS). The following day, a 2 ml of transfection mixture containing lentiviral packaging plasmids such as 7.5 μg of pMD2.G (Addgene, #12259), 11.4 μg of pMDLg-RRE (Addgene, #12251), 5.4 μg of pRSV-REV (Addgene, #12253), and 13.7 μg of SATT plasmid with 114 μl of PEI (1 mg/ml) was prepared in 150 mM NaCl.

After vortexing, solutions were incubated 10 min at room temperature (RT) before adding to the HEK cells. The day after transfection, culture medium was changed by fresh DMEM/FBS/penicillin (Pen)/streptomycin (Strep). Three days after transfection, lentiviral suspension was harvested by filtering through a 0.45-μm syringe filter (PN4184, Pall Corporation). Lentiviral particle concentration was determined using the HIV Type 1 p24 antigen ELISA Kit (ZeptoMetrix Corporation).

Generation of SATT-, GFP-LAZSUL–, and NSMCE2-rescued cell lines

U2OS cells were seeded in plates with a diameter of 15 cm at 10% confluency with DMEM + 10% FBS. The next day, cell culture medium was replaced with either lentiviral SATT-, GFP-LAZSUL–, or NSMCE2-rescued constructs containing medium and polybrene (8 μg/ml). Lentivirus containing medium was replaced by fresh DMEM/FBS/Pen/Strep culture medium after 24 hours. After 2 days in fresh medium, specific antibiotics were added to select positive clones. Puromycin (3 μg/ml) was added to the medium for selection of SATT- and GFP-LAZSUL–positive clones. Blasticidin (10 μg/ml) was used in the case of the NSMCE2 wild-type– and mutant-rescued cells.

shPIAS4 transduction for PIAS4 knockdown

Transductions were performed in DMEM containing polybrene (8 μg/ml) either with PIAS4 or a control nontargeting shRNA. Cells were infected with a multiplicity of infection of 3 with third generation lentiviruses encoding shRNA. DMEM containing virus was replaced after 24 hours of infection. Cells were harvested and lysed 3 days after infection. Plasmids used for shRNA-mediated knockdown were derived from the MISSION shRNA library (Sigma-Aldrich) with number TRCN0000004115 (shPIAS4) and SHC-002 (shControl).

Cell culture

U2OS (RRID: CVCL_0042) and HEK 293T (RRID: CVCL_0063) cells were cultured in DMEM supplemented with 10% FBS and Pen (100 U/ml)/Strep (100 μg/ml) at 37°C and 5% CO_2 unless specified. Cells were regularly tested for mycoplasma contamination.

Anti-SUMO1 and SUMO2/3 immunostaining

Cells were grown on 9-mm coverslips and fixed with 1% paraformaldehyde (PFA) and 0.3% Triton X-100 for 20 min at RT. A second round was performed with 1% PFA, 0.3% Triton X-100, and 0.5% methanol for 20 min at RT. Next, cells were washed three times with phosphate-buffered saline (PBS) and then blocked for 30 min with 0.5% blocking reagent (Roche) in 0.1 M tris (pH 7.5) and 0.15 M NaCl (TNB). Cells were then incubated with either anti-SUMO1 or anti-SUMO2/3 antibody in TNB for 1 hour. Coverslips were washed five times with PBS and incubated with the secondary antibody (goat anti-mouse coupled to Alexa Fluor594) in TNB for 1 hour. Next, coverslips were washed five times with PBS and mounted onto a microscopy slide using citifluor/4′,6-diamidino-2-phenylindole solution (500 ng/ml). Immunofluorescence image analysis was performed using the FiJi-ImageJ distribution (*50*).

Generation of His-SUMO1 and His-SUMO2 $_{Q87R}$ U2OS cell lines

U2OS cells were infected using a bicistronic lentivirus encoding either a 10xHis-SUMO1-IRES-GFP or a 10xHis-SUMO2$_{Q87R}$-IRES-GFP separated by an internal ribosomal entry site (IRES), which was modified from previously described 10xHis-SUMO2-WT (*51*). Following infection, U2OS cells were sorted in an FACSAria III (BD Biosciences) for low GFP levels.

Purification of 10xHis-SUMO1, 10xHis-SUMO2 $_{Q87R}$, and SATT conjugates

Following the TULIP2 methodology (*15*), five 15-cm-diameter plates of U2OS control cells or expressing 10xHis-SUMO1, 10xHis-SUMO2$_{Q87R}$, or a particular SATT were grown up to 60 to 80% confluence. Expression of SATTs constructs was induced with doxycycline (1 μg/ml) once 60 to 80% confluency was reached. Twenty-four hours after doxycycline induction, cells were treated with proteasome inhibitor MG132 (Sigma-Aldrich) at 10 μM for 5 hours. After proteasome inhibition, cells were washed twice with ice-cold PBS and scraped. Cells were spun down and collected in 2 ml of ice-cold PBS, and 100 μl of sample was taken as input and lysed in 200 μl of SNTBS buffer [2% SDS, 1% NP-40, 50 mM tris (pH 7.5), and 150 mM NaCl]. After additional centrifugation, cells were lysed in 10 ml of guanidinium buffer [6 M guanidine-HCl, 0.1 M sodium phosphate, and 10 mM tris (pH 7.8)] and snap-frozen in liquid nitrogen.

After thawing, lysates were homogenized at RT by sonication at 80% amplitude during 5 s using a tip sonicator (Q125 Sonicator, QSonica, Newtown, USA). Sonication was performed twice. Subsequently, protein concentration was determined by bicinchoninic acid protein assay reagent (Thermo Fisher Scientific). Total protein in cell lysates was equalized accordingly. After equalization, cell lysates were supplemented with 5 mM β-mercaptoethanol and 50 mM imidazole (pH 8.0). Dry Ni-NTA agarose beads (100 μl; QIAGEN) were equilibrated with guanidinium buffer supplemented with 5 mM β-mercaptoethanol and 50 mM imidazole (pH 8.0). Equilibrated Ni-NTA beads were added to the cell lysates and incubated overnight at 4°C under rotation.

After lysate bead incubation, Ni-NTA beads were spun down and transferred with wash buffer 1 [6 M guanidine-HCl, 0.1 M sodium phosphate, 10 mM tris, 10 mM imidazole, 5 mM β-mercaptoethanol, and 0.2% Triton X-100 (pH 7.8)] to an Eppendorf LoBind tube (Eppendorf). After mixing and spinning down again, the beads were moved to a new LoBind tube with wash buffer 2 [8 M urea, 0.1 M sodium phosphate, 10 mM tris, 10 mM imidazole, and 5 mM β-mercaptoethanol (pH 8)]. This procedure was repeated with wash buffer 3 [8 M urea, 0.1 M sodium phosphate, 10 mM tris, 10 mM imidazole, and 5 mM β-mercaptoethanol (pH 6.3)]. Ultimately, beads were washed twice with wash buffer 4 [8 M urea, 0.1 M sodium phosphate, 10 mM tris, and 5 mM β-mercaptoethanol (pH 6.3)]. When washing with wash buffer 3 and 4, beads were allowed to equilibrate with the buffer for 15 min under rotation. For the analysis by immunoblotting, the beads were heated at 99°C for 10 min with 2x lithium dodecyl sulfate (LDS) NuPAGE sample buffer (Invitrogen).

Trypsin digestion of SATT-purified conjugates

After the final wash with wash buffer 4, Ni-NTA beads were resuspended in 7 M urea, 0.1 M NaH_2PO_4/Na_2HPO_4, and 0.01 M tris/

HCl (pH 7) and digested with 500 ng of recombinant Lys-C (Promega) at RT while shaking at 1400 rpm. After 5 hours with Lys-C, urea buffer was diluted to <2 M by adding 50 mM ATP-binding cassette. A second digestion was performed o/n at 37°C while shaking at 1400 rpm using 500 ng of sequencing grade–modified trypsin (Promega). Trypsin-digested peptides were separated from Ni-NTA beads by filtering through a 0.45-μm filter Ultrafree-MC-HV spin column (Merck Millipore).

MS sample preparation

Digested peptides were acidified by adding 2% trifluoroacetic acid. Subsequently, peptides were desalted and concentrated on triple-disc C18 stage tips as previously described (*52*). Stage tips were in-house assembled using 200-μl micro pipet tips and C18 matrix. Stage tips were activated by passing through 100 μl of methanol. Subsequently, 100 μl of buffer B (80% acetonitrile and 0.1% formic acid), 100 μl of buffer A (0.1% formic acid), the acidified peptide sample, and two times 100 μl of buffer A were passed through the stage tip. Elution was performed in 50 μl of 32.5% acetonitrile and 0.1% formic acid.

Samples were vacuum-dried using a SpeedVac RC10.10 (Jouan, France) and stored at −20°C. Before MS analysis, samples were reconstituted in 10 μl of 0.1% formic acid and transferred to autoload vials.

LC-MS/MS analysis

All the experiments were analyzed by on-line C18 nano–high-performance liquid chromatography (HPLC) MS/MS with a system consisting of an Ultimate3000 nano-gradient HPLC system (Thermo Fisher Scientific, Bremen, Germany) and an Exploris480 mass spectrometer (Thermo Fisher Scientific, Bremen, Germany). Samples were injected onto a cartridge precolumn (300 μm by 5 mm; C18 PepMap, 5 μm, 100 A) with a flow of 10 μl/min for 3 min (Thermo Fisher Scientific, Bremen, Germany) and eluted via a homemade analytical nano-HPLC column (50 cm by 75 μm; Reprosil-Pur C18-AQ 1.9 μm, 120 A) (Dr. Maisch, Ammerbuch, Germany). The gradient was run from 2 to 38% solvent B (80% acetonitrile and 0.1% formic acid) in 120 min. The nano-HPLC column was drawn to a tip of ~10 μm and acted as the electrospray needle of the MS source. The temperature of the nano-HPLC column was set to 50°C (Sonation GmbH, Biberach, Germany). The mass spectrometer was operated in data-dependent MS/MS mode for a cycle time of 3 s, with a higher energy collision dissociation (HCD) collision energy at 28 V and recording of the MS2 spectrum in the Orbitrap, with a quadrupole isolation width of 1.2 Da. In the master scan (MS1), the resolution was 120,000, the scan range of 350 to 1600, at a standard automatic gain control (AGC) target with maximum fill time of 50 ms. A lock mass correction on the background ion mass/charge ratio = 445.12 was used. Precursors were dynamically excluded after $n = 1$ with an exclusion duration of 45 s and with a precursor range of 10 parts per million. Charge states 2 to 5 were included. For MS2, the scan range mode was set to automated, and the MS2 scan resolution was 30,000 at a normalized AGC target of 100% with a maximum fill time of 60 ms.

MS data analysis

All raw data was analyzed using MaxQuant (version 1.6.14) as previously described (*53*). We performed two searches, first one analyzing the U2OS samples, HIS-SUMO1 and SUMO1 SATTs and the other one analyzing U2OS, HIS-SUMO2$_{Q87R}$, and SUMO2$_{Q87R}$ SATTs. We performed the search against an in silico digested UniProt reference proteome for *Homo sapiens* including canonical and isoform sequences (5 July 2021). Database searches were performed according to standard settings with the following modifications: Digestion with trypsin/P was used, allowing four missed cleavages. Oxidation (M), acetyl (protein N-term), phospho (S, T), and, in the SUMO2$_{Q87R}$ SATTs analysis, also QQTGG (K) (for SUMOylation sites) were allowed as variable modifications with a maximum number of 3. Carbamidomethyl (C) was disabled for SATTs analysis as a fixed modification. Label-free quantification (LFQ) was enabled, not allowing Fast LFQ. At least two peptides were needed to be identified to calculate LFQ for a protein. All peptides were used for protein quantification.

Output from the analysis in MaxQuant was further processed in the Perseus computational platform version 1.6.14 (*54*) for statistical analysis. LFQ values were $\log_2$- transformed, and contaminants, proteins identified by site and reverse peptides, were excluded from the analysis. Next, samples were separated in two packages. The first package consisted of U2OS control samples and HIS-SUMO samples, and the second package consisted of the SATT samples. The first package was analyzed to determine which proteins could be statistically considered a HIS-SUMO target. Proteins that were not identified in at least four biological replicates of at least one condition were removed. Then, missing values were imputed from a normal distribution with a width of 0.3 and a downshift of 2.5, which resulted in a percentage of imputed valid values of 29.7% (data S3), 39.7% (data S4), 7.6% (data S6), and 11.8% (data S7). We performed *t* test corrected with a false discovery rate (FDR) = 0.05 and S0 = 0.1. Statistically enriched proteins were considered HIS-SUMO substrates (data S1 and S2). Next, we proceeded only considering proteins that were HIS-SUMO substrates and merge the table with package 2 samples (left sided), so only proteins that were HIS-SUMO substrates remained in the datasets. For the unbiased analysis, this step was omitted. Each SATT set was independently analyzed as performed with U2OS and HIS-SUMO samples. Last, all the analyses were merged and exported and further processed in Microsoft Excel 365 for comprehensive data visualization and calculation of SATT indexes. For the heatmaps, the ΔGG and Mut samples were removed and the *z* score was calculated for heatmap visualization.

Similarly, for the NSMCE2-KO orthogonal validation, LFQ values were $\log_2$-transformed, and contaminants, proteins identified by site and reverse peptides, were excluded from the analysis. Proteins that were not identified in at least four biological replicates of at least one condition were removed. Then, missing values were imputed from a normal distribution with a width of 0.3 and a downshift of 2.5. Groups comparisons were performed by *t* test with an FDR = 0.05 and S0 = 0.1, and the data were exported into Microsoft Excel 365 for comprehensive data browsing.

Gene Ontology analysis

Gene Ontology analyses from the SATT substrates were performed using the PANTHER overrepresentation test (released 13 October 2022) from the Gene Ontology Consortium (*55*). The Gene Ontology Database used was released on 11 July 2022, and the test was a Fisher's test with Bonferroni correction. The whole human proteome was used as reference for comparison.

Electrophoresis and immunoblotting

Samples were separated on Novex 4 to 12% gradient gels (Thermo Fisher Scientific) using NuPAGE Mops SDS running buffer [50 mM Mops, 50 mM tris base, 0.1% SDS, and 1 mM EDTA (pH 7.7)] and transferred onto Amersham Protran Premium 0.45 NC nitrocellulose blotting membranes (GE Healthcare) using a Bolt Mini-Gel system (Thermo Fisher Scientific), which was used for both the gel electrophoresis and the protein transfer to the membrane according to vendor's instructions. Membranes were stained with Ponceau-S (Sigma-Aldrich) to determine the total amount of protein loaded. Next, membranes were blocked with blocking solution (8% Elk milk and 0.1% Tween 20 in PBS) for 1 hour before primary antibody incubation. Chemiluminescence reaction was initiated with Western Bright Quantum Western blotting detection kit (Advansta-Isogen) and measured in a ChemiDoc imaging system (Bio-Rad, Hercules, CA, USA).

ZMIZ2 in vitro SUMOylation assay

ZMIZ2 was purified from *Escherichia coli* cells transformed with pGEX-6P-3_GST-FLAG-ZIMP7 (419-920). Expression was induced by adding 0.25 mM isopropyl-β-D-thiogalactopyranoside in the induction buffer (20 mM Hepes, 1 mM $MgCl_2$, and 0.05% glucose) for 5 hours and 30 m.

After induction and harvesting, cells were resuspended in PBS with 0.5 M NaCl/1 mM phenylmethylsulfonyl fluoride (PMSF) supplemented with protease inhibitor (PI) and sonicated and then sonicated again in the presence of Triton X-100. After spin down, soluble fraction was incubated with glutathione *S*-transferase (GST) beads for 2 hours at 4°C. Beads were washed twice with PBS supplemented with 0.5 M NaCL/1 mM PMSF and PI without EDTA and three times with 50 mM tris (pH 7.5)/0.5 M NaCl. Beads were eluted with 20 mM glutathione in the same buffer twice for 10 min.

Recombinant SUMOylation machinery (*56*), including 300 ng of E1, 0/100/200 ng of E2, 4 μg of SUMO1/SUMO2, and 0/300 of ng ZMIZ2, was incubated for 3 hours at 37°C in in vitro SUMOylation buffer [50 mM tris (pH 7.5), 2 mM $ZnCl_2$ with PI cocktail without EDTA (11836170001, Roche) and energy regeneration solution of 1:25 (B-10, Boston Biochem)] in a total volume of 25 μl. SUMO chain formation was analyzed by immunoblotting.

Data representation

Super plots were constructed using SuperPlotsOfData (*57*). For the SATT polar plots, a web app for the display of multiple volcano plots side-by-side, named polarVolcaNoseR, was made with R/Shiny.

The code was written using R (www.r-project.org) and Rstudio (www.rstudio.com). To run the app, several freely available packages are required: shiny, ggplot2, magrittr, dplyr, ggrepel, htmlwidgets, ggiraph, glue, and scales. The web app is freely accessible at https://amsterdamstudygroup.shinyapps.io/PolaRVolcaNoseR/, and the code is available at github (https://github.com/ScienceParkStudyGroup/polarVolcaNoseR). In the default "polar" representation, the volcano plots are plotted in a circle, where the radius depicts the $-\log_{10}(P \text{ value})$ and the circumference reflects the positive $\log_2$(fold change). Labels of proteins can be added by point and click, and the data of individual dots are displayed when the cursor hovers over a data point. A customized interactive plot can be exported as an HTML file.

Supplementary Materials

This PDF file includes:
Tables S1 and S2
Figs. S1 to S6
Legends for data S1 to S14

Other Supplementary Material for this manuscript includes the following:
Data S1 to S14

REFERENCES AND NOTES

1. G. Duan, D. Walther, The roles of post-translational modifications in the context of protein interaction networks. *PLOS Comput. Biol.* **11**, e1004049 (2015).
2. D. Salas-Lloret, R. Gonzalez-Prieto, Insights in post-translational modifications: Ubiquitin and SUMO. *Int. J. Mol. Sci.* **23**, 3281 (2022).
3. F. Trulsson, A. C. O. Vertegaal, Site-specific proteomic strategies to identify ubiquitin and SUMO modifications: Challenges and opportunities. *Semin Cell Dev. Biol.* **132**, 97–108 (2022).
4. V. Akimov, I. Barrio-Hernandez, S. V. F. Hansen, P. Hallenborg, A.-K. Pedersen, D. B. Bekker-Jensen, M. Puglia, S. D. K. Christensen, J. T. Vanselow, M. M. Nielsen, I. Kratchmarova, C. D. Kelstrup, J. V. Olsen, B. Blagoev, UbiSite approach for comprehensive mapping of lysine and N-terminal ubiquitination sites. *Nat. Struct. Mol. Biol.* **25**, 631–640 (2018).
5. F. Trulsson, V. Akimov, M. Robu, N. van Overbeek, D. A. P. Berrocal, R. G. Shah, J. Cox, G. M. Shah, B. Blagoev, A. C. O. Vertegaal, Deubiquitinating enzymes and the proteasome regulate preferential sets of ubiquitin substrates. *Nat. Commun.* **13**, 2736 (2022).
6. I. A. Hendriks, D. Lyon, D. Su, N. H. Skotte, J. A. Daniel, L. J. Jensen, M. L. Nielsen, Site-specific characterization of endogenous SUMOylation across species and organs. *Nat. Commun.* **9**, 2456 (2018).
7. I. A. Hendriks, D. Lyon, C. Young, L. J. Jensen, A. C. O. Vertegaal, M. L. Nielsen, Site-specific mapping of the human SUMO proteome reveals co-modification with phosphorylation. *Nat. Struct. Mol. Biol.* **24**, 325–336 (2017).
8. I. A. Hendriks, R. C. J. D'Souza, B. Yang, M. Verlaan-de Vries, M. Mann, A. C. O. Vertegaal, Uncovering global SUMOylation signaling networks in a site-specific manner. *Nat. Struct. Mol. Biol.* **21**, 927–936 (2014).
9. F. Impens, L. Radoshevich, P. Cossart, D. Ribet, Mapping of SUMO sites and analysis of SUMOylation changes induced by external stimuli. *Proc. Natl. Acad. Sci. U.S.A.* **111**, 12432–12437 (2014).
10. R. Gonzalez-Prieto, K. Eifler-Olivi, L. A. Claessens, E. Willemstein, Z. Xiao, C. M. P. Talavera Ormeno, H. Ovaa, H. D. Ulrich, A. C. O. Vertegaal, Global non-covalent SUMO interaction networks reveal SUMO-dependent stabilization of the non-homologous end joining complex. *Cell Rep.* **34**, 108691 (2021).
11. C. Li, F. P. McManus, C. Plutoni, C. M. Pascariu, T. Nelson, L. E. Alberici Delsin, G. Emery, P. Thibault, Quantitative SUMO proteomics identifies PIAS1 substrates involved in cell migration and motility. *Nat. Commun.* **11**, 834 (2020).
12. I. Uzoma, J. Hu, E. Cox, S. Xia, J. Zhou, H.S. Rho, C. Guzzo, C. Paul, O. Ajala, C.R. Goodwin, J. Jeong, C. Moore, H. Zhang, P. Meluh, S. Blackshaw, M. Matunis, J. Qian, H. Zhu, Global identification of small ubiquitin-related modifier (SUMO) substrates reveals crosstalk between SUMOylation and phosphorylation promotes cell migration. *Mol. Cell. Proteomics* **17**, 871–888 (2018).
13. H. F. O'Connor, N. Lyon, J. W. Leung, P. Agarwal, C. D. Swaim, K. M. Miller, J. M. Huibregtse, Ubiquitin-Activated Interaction Traps (UBAITs) identify E3 ligase binding partners. *EMBO Rep.* **16**, 1699–1712 (2015).
14. R. González-Prieto, A. C. O. Vertegaal, in *SUMOylation and Ubiquitination: Current and Emerging Concepts*, V. G. Wilson, Ed. (Caister Academic Press, 2019), chap. 10, pp. 147–160.
15. D. Salas-Lloret, G. Agabitini, R. Gonzalez-Prieto, TULIP2: An improved method for the identification of ubiquitin E3-specific targets. *Front. Chem.* **7**, 802 (2019).
16. R. Kumar, R. Gonzalez-Prieto, Z. Xiao, M. Verlaan-de Vries, A. C. O. Vertegaal, The STUbL RNF4 regulates protein group SUMOylation by targeting the SUMO conjugation machinery. *Nat. Commun.* **8**, 1809 (2017).
17. R. Moreno-Ayala, D. Schnabel, E. Salas-Vidal, H. Lomeli, PIAS-like protein Zimp7 is required for the restriction of the zebrafish organizer and mesoderm development. *Dev. Biol.* **403**, 89–100 (2015).
18. Y. Peng, J. Lee, C. Zhu, Z. Sun, A novel role for protein inhibitor of activated STAT (PIAS) proteins in modulating the activity of Zimp7, a novel PIAS-like protein, in androgen receptor-mediated transcription. *J. Biol. Chem.* **285**, 11465–11475 (2010).
19. J. Beliakoff, Z. Sun, Zimp7 and Zimp10, two novel PIAS-like proteins, function as androgen receptor coregulators. *Nucl. Recept. Signal.* **4**, e017 (2006).

20. H. Lomeli, ZMIZ proteins: Partners in transcriptional regulation and risk factors for human disease. *J. Mol. Med. (Berl)* **100**, 973–983 (2022).
21. M. H. Tatham, M.-C. Geoffroy, L. Shen, A. Plechanovova, N. Hattersley, E. G. Jaffray, J. J. Palvimo, R. T. Hay, RNF4 is a poly-SUMO-specific E3 ubiquitin ligase required for arsenic-induced PML degradation. *Nat. Cell Biol.* **10**, 538–546 (2008).
22. L. Cappadocia, A. Pichler, C. D. Lima, Structural basis for catalytic activation by the human ZNF451 SUMO E3 ligase. *Nat. Struct. Mol. Biol.* **22**, 968–975 (2015).
23. N. Eisenhardt, V. K. Chaugule, S. Koidl, M. Droescher, E. Dogan, J. Rettich, P. Sutinen, S. Y. Imanishi, K. Hofmann, J. J. Palvimo, A. Pichler, A new vertebrate SUMO enzyme family reveals insights into SUMO-chain assembly. *Nat. Struct. Mol. Biol.* **22**, 959–967 (2015).
24. L. Wang, C. Wansleeben, S. Zhao, P. Miao, W. Paschen, W. Yang, SUMO2 is essential while SUMO3 is dispensable for mouse embryonic development. *EMBO Rep.* **15**, 878–885 (2014).
25. Y. Galanty, R. Belotserkovskaya, J. Coates, S. Polo, K. M. Miller, S. P. Jackson, Mammalian SUMO E3-ligases PIAS1 and PIAS4 promote responses to DNA double-strand breaks. *Nature* **462**, 935–939 (2009).
26. N. Varejao, E. Ibars, J. Lascorz, N. Colomina, J. Torres-Rosell, D. Reverter, DNA activates the Nse2/Mms21 SUMO E3 ligase in the Smc5/6 complex. *EMBO J.* **37**, e98306 (2018).
27. M. Agostinho, V. Santos, F. Ferreira, R. Costa, J. Cardoso, I. Pinheiro, J. Rino, E. Jaffray, R. T. Hay, J. Ferreira, Conjugation of human topoisomerase 2 α with small ubiquitin-like modifiers 2/3 in response to topoisomerase inhibitors: Cell cycle stage and chromosome domain specificity. *Cancer Res.* **68**, 2409–2418 (2008).
28. M. J. Schellenberg, J. A. Lieberman, A. Herrero-Ruiz, L. R. Butler, J. G. Williams, A. M. Muñoz-Cabello, G. A. Mueller, R. E. London, F. Cortés-Ledesma, R. S. Williams, ZATT (ZNF451)-mediated resolution of topoisomerase 2 DNA-protein cross-links. *Science* **357**, 1412–1416 (2017).
29. J. Liang, B.-Z. Li, A. P. Tan, R. D. Kolodner, C. D. Putnam, H. Zhou, SUMO E3 ligase Mms21 prevents spontaneous DNA damage induced genome rearrangements. *PLOS Genet.* **14**, e1007250 (2018).
30. Y. Sun, L. M. Miller Jenkins, Y. P. Su, K. C. Nitiss, J. L. Nitiss, Y. Pommier, A conserved SUMO pathway repairs topoisomerase DNA-protein cross-links by engaging ubiquitin-mediated proteasomal degradation. *Sci. Adv.* **6**, eaba6290 (2020).
31. P. Sarangi, X. Zhao, SUMO-mediated regulation of DNA damage repair and responses. *Trends Biochem. Sci.* **40**, 233–242 (2015).
32. S. Dabir, A. Kluge, A. Dowlati, The association and nuclear translocation of the PIAS3-STAT3 complex is ligand and time dependent. *Mol. Cancer Res.* **7**, 1854–1860 (2009).
33. M. Sundvall, A. Korhonen, K. Vaparanta, J. Anckar, K. Halkilahti, Z. Salah, R. I. Aqeilan, J. J. Palvimo, L. Sistonen, K. Elenius, Protein inhibitor of activated STAT3 (PIAS3) protein promotes SUMOylation and nuclear sequestration of the intracellular domain of ErbB4 protein. *J. Biol. Chem.* **287**, 23216–23226 (2012).
34. J.-H. Man, H.-Y. Li, P.-J. Zhang, T. Zhou, K. He, X. Pan, B. Liang, A.-L. Li, J. Zhao, W.-L. Gong, B.-F. Jin, Q. Xia, M. Yu, B.-F. Shen, X.-M. Zhang, PIAS3 induction of PRB sumoylation represses PRB transactivation by destabilizing its retention in the nucleus. *Nucleic Acids Res.* **34**, 5552–5566 (2006).
35. M. H. Tatham, E. Jaffray, O. A. Vaughan, J. M. Desterro, C. H. Botting, J. H. Naismith, R. T. Hay, Polymeric chains of SUMO-2 and SUMO-3 are conjugated to protein substrates by SAE1/SAE2 and Ubc9. *J. Biol. Chem.* **276**, 35368–35374 (2001).
36. D. E. Verver, Y. Zheng, D. Speijer, R. Hoebe, H. L. Dekker, S. Repping, J. Stap, G. Hamer, Non-SMC element 2 (NSMCE2) of the SMC5/6 complex helps to resolve topological stress. *Int. J. Mol. Sci.* **17**, 1782 (2016).
37. A. Jacome, P. Gutierrez-Martinez, F. Schiavoni, E. Tenaglia, P. Martinez, S. Rodríguez-Acebes, E. Lecona, M. Murga, J. Méndez, M. A. Blasco, O. Fernandez-Capetillo, NSMCE2 suppresses cancer and aging in mice independently of its SUMO ligase activity. *EMBO J.* **34**, 2604–2619 (2015).
38. D. B. Krastev, S. Li, Y. Sun, A. J. Wicks, G. Hoslett, D. Weekes, L. M. Badder, E. G. Knight, R. Marlow, M. C. Pardo, L. Yu, T. T. Talele, J. Bartek, J. S. Choudhary, Y. Pommier, S. J. Pettitt, A. N. J. Tutt, K. Ramadan, C. J. Lord, The ubiquitin-dependent ATPase p97 removes cytotoxic trapped PARP1 from chromatin. *Nat. Cell Biol.* **24**, 62–73 (2022).
39. D. Lee, K. Apelt, S.-O. Lee, H.-R. Chan, M. S. Luijsterburg, J. W. C. Leung, K. M. Miller, ZMYM2 restricts 53BP1 at DNA double-strand breaks to favor BRCA1 loading and homologous recombination. *Nucleic Acids Res.* **50**, 3922–3943 (2022).
40. J. Schimmel, K. M. Larsen, I. Matic, M. van Hagen, J. Cox, M. Mann, J. S. Andersen, A. C. O. Vertegaal, The ubiquitin-proteasome system is a key component of the SUMO-2/3 cycle. *Mol. Cell. Proteomics* **7**, 2107–2122 (2008).
41. R. Gonzalez-Prieto, S. A. Cuijpers, R. Kumar, I. A. Hendriks, A. C. Vertegaal, c-Myc is targeted to the proteasome for degradation in a SUMOylation-dependent manner, regulated by PIAS1, SENP7 and RNF4. *Cell Cycle* **14**, 1859–1872 (2015).
42. A. M. Sriramachandran, K. Meyer-Teschendorf, S. Pabst, H. D. Ulrich, N. H. Gehring, K. Hofmann, G. J. K. Praefcke, R. J. Dohmen, Arkadia/RNF111 is a SUMO-targeted ubiquitin ligase with preference for substrates marked with SUMO1-capped SUMO2/3 chain. *Nat. Commun.* **10**, 3678 (2019).
43. A. Seifert, P. Schofield, G. J. Barton, R. T. Hay, Proteotoxic stress reprograms the chromatin landscape of SUMO modification. *Sci. Signal.* **8**, rs7 (2015).
44. J. J. Palecek, SMC5/6: Multifunctional player in replication. *Genes (Basel)* **10**, **7** (2019).
45. C. Li, A. Boutet, C. M. Pascariu, T. Nelson, M. Courcelles, Z. Wu, S. Comtois-Marotte, G. Emery, P. Thibault, SUMO proteomics analyses identify protein inhibitor of activated STAT-mediated regulatory networks involved in cell cycle and cell proliferation. *J. Proteome Res.* **22**, 812–825 (2023).
46. I. A. Hendriks, R. C. D'Souza, J. G. Chang, M. Mann, A. C. Vertegaal, System-wide identification of wild-type SUMO-2 conjugation sites. *Nat. Commun.* **6**, 7289 (2015).
47. J. Schimmel, K. Eifler, J. O. Sigurðsson, S. A. G. Cuijpers, I. A. Hendriks, M. Verlaan-de Vries, C. D. Kelstrup, C. Francavilla, R. H. Medema, J. V. Olsen, A. C. O. Vertegaal, Uncovering SUMOylation dynamics during cell-cycle progression reveals FoxM1 as a key mitotic SUMO target protein. *Mol. Cell* **53**, 1053–1066 (2014).
48. P. Gonzalez-Rodriguez, E. Zampese, K. A. Stout, J. N. Guzman, E. Ilijic, B. Yang, T. Tkatch, M. A. Stavarache, D. L. Wokosin, L. Gao, M. G. Kaplitt, J. López-Barneo, P. T. Schumacker, D. J. Surmeier, Disruption of mitochondrial complex I induces progressive parkinsonism. *Nature* **599**, 650–656 (2021).
49. J. Magalhaes, E. Tresse, P. Ejlerskov, E. Hu, Y. Liu, A. Marin, A. Montalant, L. Satriano, C. F. Rundsten, E. M. M. Carlsen, R. Rydbirk, A. Sharifi-Zarchi, J. B. Andersen, S. Aznar, T. Brudek, K. Khodosevich, M. Prinz, J.F. M. Perrier, M. Sharma, T. Gasser, S. Issazadeh-Navikas, PIAS2-mediated blockade of IFN-β signaling: A basis for sporadic Parkinson disease dementia. *Mol. Psychiatry* **26**, 6083–6099 (2021).
50. J. Schindelin, I. Arganda-Carreras, E. Frise, V. Kaynig, M. Longair, T. Pietzsch, S. Preibisch, C. Rueden, S. Saalfeld, B. Schmid, J.Y. Tinevez, D. J. White, V. Hartenstein, K. Eliceiri, P. Tomancak, A. Cardona, Fiji: An open-source platform for biological-image analysis. *Nat. Methods* **9**, 676–682 (2012).
51. Z. Xiao, J.-G. Chang, I. A. Hendriks, J. O. Sigurðsson, J. V. Olsen, A. C. O. Vertegaal, System-wide analysis of SUMOylation dynamics in response to replication stress reveals novel small ubiquitin-like modified target proteins and acceptor lysines relevant for genome stability. *Mol. Cell. Proteomics* **14**, 1419–1434 (2015).
52. J. Rappsilber, M. Mann, Y. Ishihama, Protocol for micro-purification, enrichment, pre-fractionation and storage of peptides for proteomics using StageTips. *Nat. Protoc.* **2**, 1896–1906 (2007).
53. S. Tyanova, T. Temu, J. Cox, The MaxQuant computational platform for mass spectrometry-based shotgun proteomics. *Nat. Protoc.* **11**, 2301–2319 (2016).
54. S. Tyanova, T. Temu, P. Sinitcyn, A. Carlson, M. Y. Hein, T. Geiger, M. Mann, J. Cox, The Perseus computational platform for comprehensive analysis of (prote)omics data. *Nat. Methods* **13**, 731–740 (2016).
55. H. Mi, D. Ebert, A. Muruganujan, C. Mills, L.-P. Albou, T. Mushayamaha, P. D. Thomas, PANTHER version 16: A revised family classification, tree-based classification tool, enhancer regions and extensive API. *Nucleic Acids Res.* **49**, D394–D403 (2021).
56. K. Eifler, S. A. G. Cuijpers, E. Willemstein, J. A. Raaijmakers, D. el Atmioui, H. Ovaa, R. H. Medema, A. C. O. Vertegaal, SUMO targets the APC/C to regulate transition from metaphase to anaphase. *Nat. Commun.* **9**, 1119 (2018).
57. J. Goedhart, SuperPlotsOfData-a web app for the transparent display and quantitative comparison of continuous data from different conditions. *Mol. Biol. Cell* **32**, 470–474 (2021).
58. Y. Perez-Riverol, A. Csordas, J. Bai, M. Bernal-Llinares, S. Hewapathirana, D. J. Kundu, A. Inuganti, J. Griss, G. Mayer, M. Eisenacher, E. Pérez, J. Uszkoreit, J. Pfeuffer, T. Sachsenberg, Ş. Yılmaz, S. Tiwary, J. Cox, E. Audain, M. Walzer, A. F. Jarnuczak, T. Ternent, A. Brazma, J. A. Vizcaíno, The PRIDE database and related tools and resources in 2019: Improving support for quantification data. *Nucleic Acids Res.* **47**, D442–D450 (2019).

Acknowledgments: Authors would like to thank G. Hamer for sharing Parental and NSMCE2-KO U2OS cell lines and H. van Attikum and M. Dijk for sharing the pGEX-6P-3_GST-FLAG-ZIMP7 plasmid. **Funding:** For research and publication of this article, this work was supported by the Spanish Ministry of Science and Innovation, the Spanish Research Agency, and the European Regional Development Fund. Proyecto PID2021-122361NA-I00 financiado por MCIN/AEI/10.13039/501100011033/ y por FEDER Una manera de hacer Europa. This work was also supported by the Andalusian Regional Government, Spain, Junta de Andalucía (EMERGIA20_00276 to R.G.-P.), Dutch Cancer Society (KWF-KIG 11367/2017-2 to R.G.-P.), European Research Council (ERC grant 310913 to A.C.O.V.), Dutch Research Council (NWO; 724.016.003 to A.C.O.V.), Max Plank Society (to A.P. and E.N.), and Swiss National Science Foundation (SNSF 310030_204583 to A.P.). **Author contributions:** Conceptualization: R.G.-P., A.C.O.V., and J.G. Methodology: D.S.-L., R.G.-P., and J.G. Investigation: D.S.-L., R.G.-P., N.S.J., E.N., C.v.d.M., E.G., A.H.d.R., and H.A.M.O. Supervision: R.G.-P., A.C.O.V., A.P., P.A.v.V. Writing—original draft: R.G.-P. Writing—review and editing: D.S.-L., N.S.J., A.C.O.V., and R.G.-P. **Competing interests:** The authors declare that they have no competing interests. **Data and materials**

availability: All data needed to evaluate the conclusions in the paper are present in the paper and/or the Supplementary Materials. The MS proteomics data have been deposited to the ProteomeXchange Consortium via the PRIDE partner repository (*58*) with the dataset identifiers PXD038326. The Polar SATTs code is deposited at Zenodo (https://doi.org/10.5281/zenodo.7993831). Plasmids and cell lines generated in this study are available upon request from Dr. Román González-Prieto at roman.gonzalez@cabimer.es. The affinity purified ZNF451-3 antibody (anti-LAZSUL) is very limited, and only small aliquots of the rabbit serum can be shared.

Submitted 16 February 2023
Accepted 28 June 2023
Published 2 August 2023
10.1126/sciadv.adh2073